

# Whole-body biodistribution and radiation dosimetry in monkeys and humans of the phosphodiesterase 4 radioligand [ $^{11}\text{C}$ ](*R*)-rolipram: comparison of two-dimensional planar, bisected and quadrisected image analyses

David R. Sprague, Masahiro Fujita\*, Yong Hoon Ryu, Jeih-San Liow, Victor W. Pike, Robert B. Innis

*Molecular Imaging Branch, National Institute of Mental Health, Bethesda, MD 20892-2035, USA*

Received 6 November 2007; received in revised form 16 January 2008; accepted 11 February 2008

## Abstract

**Introduction:** [ $^{11}\text{C}$ ](*R*)-Rolipram is a selective radioligand for positron emission tomography (PET) imaging of phosphodiesterase 4, an enzyme that metabolizes 3',5'-cyclic adenosine monophosphate. The aim of this study was to estimate the human radiation absorbed dose of the radioligand based on its biodistribution in both monkeys and humans.

**Methods:** Whole-body PET images were acquired for 2 h after injecting [ $^{11}\text{C}$ ](*R*)-rolipram in eight healthy humans and three monkeys. The simple method of using a single two-dimensional (2D) planar image was compared to more time-consuming methods that used two (bisected) or four (quadrisectioned) tomographic images in the anteroposterior direction.

**Results:** Effective dose was 4.8  $\mu\text{Gy}/\text{MBq}$  based on 2D planar images. The effective dose was only slightly lower by 1% and 5% using the bisected and quadrisectioned images, respectively. Nevertheless, the two tomographic methods may have more accurately estimated the exposure of some organs (e.g., kidneys) that are asymmetrically located in the body or have radioactivity that appears to overlap on 2D planar images. Monkeys had a different biodistribution pattern compared to humans (e.g., greater urinary excretion) such that their data overestimated the effective dose in humans by 40%.

**Conclusions:** The effective dose of [ $^{11}\text{C}$ ](*R*)-rolipram was modest and comparable to that of other  $^{11}\text{C}$ -labeled radioligands. The simple and far less time-consuming 2D planar method provided accurate and somewhat more conservative estimates of effective dose than the two tomographic methods. Although monkeys are commonly used to estimate human radiation exposures, their data gave a considerable overestimation for this radioligand.

© 2008 Elsevier Inc. All rights reserved.

**Keywords:** [ $^{11}\text{C}$ ](*R*)-Rolipram; Positron emission tomography; Dosimetry; Biodistribution

## 1. Introduction

The second messenger 3',5'-cyclic adenosine monophosphate (cAMP) acts in the signal transduction of several neurotransmitters and may play an important role in psychiatric illnesses, including mood disorders [1] and drug addiction [2]. For example, the mechanism of action of several antidepressant treatments, including medications and electroconvulsive therapy, is thought to include up-

regulation of cAMP and its signal cascade [1,3–5]. Of at least 11 known families of mammalian cyclic nucleotide phosphodiesterases, phosphodiesterase 4 (PDE4) specifically metabolizes cAMP and is highly expressed in brain [6,7]. Inhibition of PDE4 would increase intracellular cAMP signaling, just like the putative mechanism of antidepressant medications. Rolipram is an inhibitor of PDE4 and, in fact, does have antidepressant effects in both animals [8,9] and humans [10]. Rolipram was, however, discontinued in clinical trials because of emetic and sedative side effects.

The more active isomer (*R*) of rolipram has been labeled with  $^{11}\text{C}$  and successfully used for positron emission

\* Corresponding author. Tel.: +1 301 451 8898; fax: +1 301 480 3610.  
E-mail address: [masahiro.fujita@nih.gov](mailto:masahiro.fujita@nih.gov) (M. Fujita).

tomography (PET) imaging in rodents [11,12], monkeys [13] and humans [14]. The radioligand has high brain uptake and low levels of nonspecific binding [15] and is a promising agent to image and to measure PDE4 in brain. The biodistribution and estimated radiation doses of [ $^{11}\text{C}$ ](*R*)-rolipram in humans have not been reported. The radiation dosimetry profile of the radioligand was partially estimated in rats [12]; however, no effective dose was estimated and only selected organ doses were listed in that report. Thus, the first aim of the present study was to determine the biokinetics and radiation safety of the radioligand through whole-body PET imaging in humans. The second aim was to compare the estimated radiation doses from two-dimensional (2D) planar, bisected and quadrisectioned images for [ $^{11}\text{C}$ ](*R*)-rolipram. As described in previous work of our laboratory, PET images obtained in this type of whole-body dosimetry study can be reinterpolated and reformatted to vary the thickness of each slice for analysis in any plane [16]. In this prior work, analysis of 2D planar or bisected images was found to estimate radiation doses more conservatively than thin-slice images for a radioligand that had a fairly broad biodistribution in the body. In addition, the report demonstrated that analysis of compressed 2D planar images resulted in considerable savings in time in comparison to minimally compressed thin-slice images without compromising the estimated radiation doses. Finally, the third aim was to determine whether results from whole-body imaging of monkeys could provide accurate estimates of radiation exposure to humans.

## 2. Materials and methods

### 2.1. Radiopharmaceutical preparation

[ $^{11}\text{C}$ ](*R*)-Rolipram was synthesized by  $^{11}\text{C}$ -methylation of (*R*)-desmethyl-rolipram using the route and method previously described by Fujita et al. [15]. Additional details are available from our Investigational New Drug application posted at <http://kidb.bioc.cwru.edu/snidd/>. For the present study, the radiochemical purity of all syntheses for both humans and monkeys ( $n=10$ ) was >99%, with average specific activities at the time of injection of  $112.3 \pm 28.2$  GBq/ $\mu\text{mol}$ . These and subsequent data are expressed as the mean  $\pm$  S.D.

### 2.2. Human subjects

The use of [ $^{11}\text{C}$ ](*R*)-rolipram in human subjects for this study was approved by the U.S. Food and Drug Administration, the Radiation Safety Committee of the National Institutes of Health and the Institutional Review Board of the National Institute of Mental Health. Eight healthy volunteers (four males and four females; mean age,  $41 \pm 9$  years; age range, 25–51 years; weight,  $89 \pm 20$  kg) who met selection criteria were enrolled in the study. Subjects provided informed written consent before completing a

screening assessment consisting of a history, physical examination, electrocardiogram and standard blood and urine analyses, including drug screening. Following the completion of PET scan, each subject repeated the complete blood count, serum chemistries and urinalysis.

### 2.3. Human PET imaging

Subjects underwent both transmission and dynamic emission scans on a GE Advance tomograph (GE Healthcare, Waukesha, WI). Following injection of  $709 \pm 79$  MBq of [ $^{11}\text{C}$ ](*R*)-rolipram, each subject was imaged in seven contiguous 15-cm bed positions beginning at the head and continuing to the middle of the thigh, following the protocol described by Sprague et al. [16].

Each subject's original tomographic PET images ( $256 \times 256$  pixels on transaxial planes) were compressed in the anteroposterior direction by summing up all activities along this direction to create three whole-body image sets: 2D planar, bisected and quadrisectioned.

1. 2D planar images. All 256 tomographic images were compressed to construct a single planar image (Fig. 1).
2. Bisected images. The 256 tomographic images were split into two sets of 128 and then compressed. In effect, this divided the body through the midcoronal plane to create anterior and posterior planar image slices.
3. Quadrisectioned images. The 256 tomographic images were examined in a sagittal view to determine the anterior and posterior limits of each subject's body within the field of view. Four sets of 40–45 contiguous tomographic slices encompassing the entire body were compressed to create four planar image slices that effectively quadrisectioned the body.

Analysis of all three image types was performed using PMOD 2.8 (pixelwise modeling computer software; PMOD Group, Adliswil, Switzerland). Source organs were those that could be visually identified on all three types of

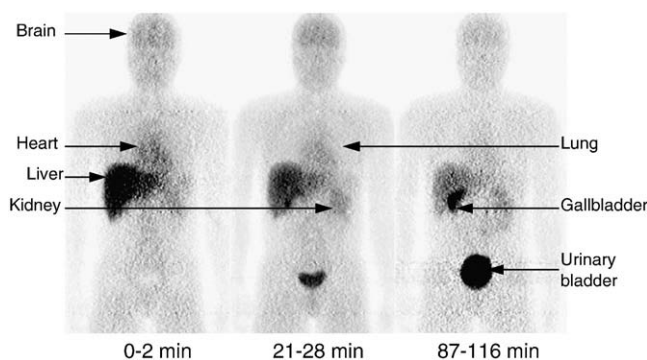


Fig. 1. Series of compressed whole-body 2D planar PET images for one healthy male. Images were obtained about 0–2, 21–28 and 87–116 min after intravenous injection of 774 MBq [ $^{11}\text{C}$ ](*R*)-rolipram. All three decay-corrected images used the same gray scale (bottom of figure).

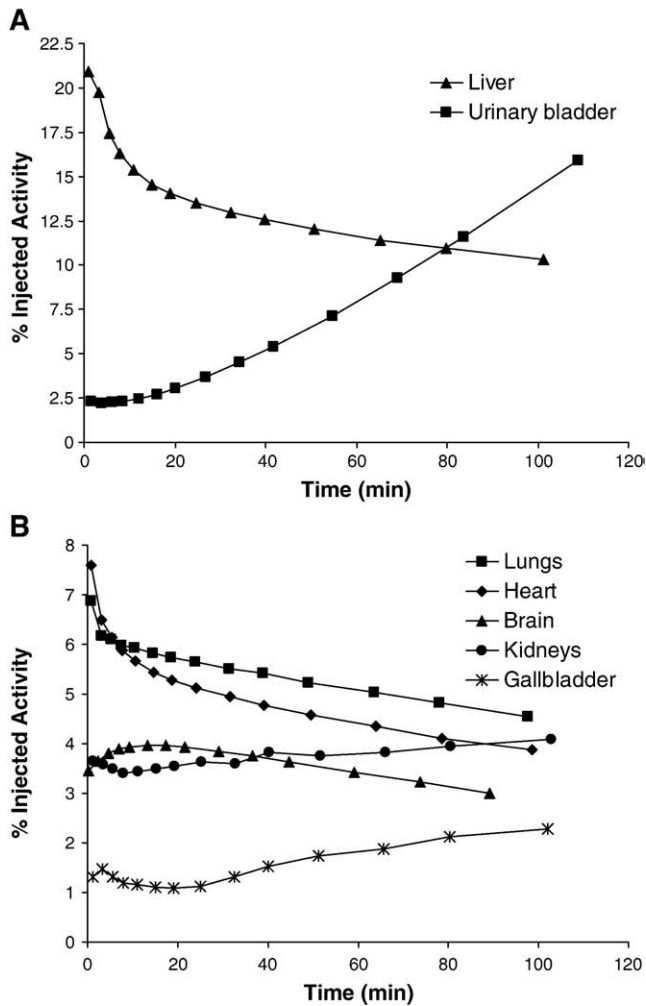


Fig. 2. Mean decay-corrected activity in visually identifiable organs that have high (A) and low (B) uptake after injection of [ $^{11}\text{C}$ ](R)-rolipram in eight human subjects. Activities were determined from 2D planar images.

images: brain, heart, lungs, liver, gallbladder, left kidney and urinary bladder. Regions of interest were drawn around each on the 2D planar images. In the case of the bisected and quadrisectioned image analyses, regions of interest were drawn around each of these structures on all of the slices in which they appeared. Uptake of activity in the heart was uniform and diffuse rather than confined solely to the myocardium. Therefore, all activity contained within the heart was designated as heart contents, not heart wall. The right kidney was not clearly distinguished, since its borders frequently overlapped liver and gallbladder. In addition, both kidneys were often difficult to identify on the 2D planar images due to diffuse overlapping activity in the abdominal cavity. Thus, the left kidney was identified on the posterior bisected images and applied to the 2D planar images. Total uptake of activity in the kidneys was calculated as twice that of the left kidney for all three image types.

#### 2.4. Animal PET imaging

Three male rhesus monkeys ( $12.6 \pm 2.4$  kg) were scanned following injection of  $282 \pm 110$  MBq [ $^{11}\text{C}$ ](R)-rolipram. To allow intubation before scanning, each monkey was anesthetized with ketamine 10–15 mg/kg im, propofol 1.2–4 mg/kg iv and glycopyrrolate 0.15–0.2 mg/kg iv. To minimize the potential effects of ketamine on PDE4 imaging, the scans started at least 90 min after its administration.

All three whole-body scans were performed on a GE Advance tomograph. The first two monkeys were scanned in four contiguous 15-cm bed positions from the top of the head to the mid-thigh. Emission scans consisted of 22 whole-body dynamic scans, and the scanning time for each bed position within a given dynamic scan increased as follows:  $4 \times 0.25$ ,  $4 \times 0.5$ ,  $8 \times 1$ ,  $4 \times 2$  and  $2 \times 4$  min. The third monkey was scanned in five contiguous 15-cm bed positions for a total of 18 dynamic scans. Individual bed positions within the dynamic scans were imaged as follows:  $2 \times 0.25$ ,  $3 \times 0.5$ ,  $6 \times 1$ ,  $5 \times 2$  and  $2 \times 4$  min. The total scanning time for both methods was about 120 min.

The 256 tomographic PET images were compressed coronally in the anteroposterior direction to create a single 2D planar image for each subject as previously described. Analysis of the images was again performed with PMOD 2.8, and regions of interest were drawn around visually identifiable source organs: brain, heart, lungs, liver, left kidney, right kidney and urinary bladder. As in human subjects, activity confined within the heart was assigned to the heart contents. Because both kidneys were visualized in animal subjects, total uptake of activity was calculated as the sum of the left and right kidneys.

#### 2.5. Residence time calculations

For each of the three methods of analysis, the uptake of activity for source organs was corrected for overall recovery of injected activity by comparing the amount of activity contained in a large region placed over the entire body to the injected activity at each time point. The activity in each source organ was multiplied by  $100/x$ , where  $x$  is the calculated percent recovery at each time point. These adjustments ensured that the uptake of activity in source organs was not underestimated. The recovery of activity averaged 88% across all time points in humans and 87% in monkeys.

Decayed activity from each source organ, including the urinary bladder, was converted to a percentage of injected activity and plotted versus time. Before creating these curves, adjustments were made to the acquisition time points for organs that were not confined to a single 15-cm bed position. Accurate mean acquisition times for these organs were obtained by weighting the time points associated with each bed position in which the organ appeared relative to the fraction of the organ's activity in each frame.

The area under an organ's decayed activity curve from time zero to infinity is equal to residence time. The

trapezoidal rule was used to calculate the area under the curve from the time of injection to the time image acquisition terminated. Any further decline in activity was assumed to occur by physical decay without any biological clearance. Please note, however, that the figures displayed herein (Figs. 2 and 4) illustrate decay-corrected activity for individual organs, since this format is more typical for PET time–activity curves. Because the cumulative urinary bladder activity could not be fitted with a suitable biexponential curve for use in a voiding bladder model, urinary bladder residence times were calculated in the same fashion as were other source organs. Residence times of all individual source organs were summed and subtracted from the fixed theoretical value of  $T_{1/2}/\ln 2=0.4906$  h to calculate the residence time of the “remainder of body” for each subject. Radiation doses were determined for each subject by entering the residence times calculated into OLINDA/EXM 1.0 (Organ Level Internal Dose Assessment/Exponential Modeling computer software; Vanderbilt University, 2003) [17] and were based on the MIRD scheme of a 70-kg adult male [18].

For monkey subjects, residence times were calculated as described above but converted into corresponding human values by multiplication with the following factor designed to scale organ and body weights:  $(o_h/b_h)/(o_m/b_m)$ , where  $o_h$  and  $o_m$  are the organ weights of human and monkey, respectively, and  $b_h$  and  $b_m$  are the body weights of human and monkey, respectively. The adjusted residence times were entered into OLINDA/EXM 1.0, and the radiation doses were again based on the model of a 70-kg human adult male.

### 3. Results

#### 3.1. Human biodistribution

Intravenous injection of [ $^{11}\text{C}$ ](R)-rolipram produced no clinically observable effects. Blood pressure, pulse, respiratory rate and ECG readings did not show any significant change from baseline measurements. In addition, blood and urine tests performed about 2.5 h after the administration of the tracer showed no significant changes from the results obtained at the subject’s initial assessment.

After injection of [ $^{11}\text{C}$ ](R)-rolipram, the brain, gallbladder, heart, kidneys, liver, lungs and urinary bladder were visually identified as source organs on 2D planar (Fig. 1), bisected and quadrisectioned image sets. The liver had the highest uptake of activity with a peak of 21% of injected activity ( $n=8$ ) on the 2D planar dataset about 1 min after injection. Peak values of radioactive uptake measured for the heart, lungs and brain were 7.6%, 6.9% and 4.0% injected activity, respectively, all occurring within 15 min of injection (Fig. 2A and B). The uptake of activity in the kidneys and gallbladder did not reach an apex during the course of the emission scans, suggesting that both hepatobiliary and renal clearance were still increasing 2 h after the administration of the tracer. The upward parabolic trend of the time–activity

curve for the urinary bladder (Fig. 2A) also indicated that urinary clearance was continuing at the end of scanning. As a result, the urinary bladder uptake could not be fitted with a mono- or biexponential curve, and a dynamic bladder model was not used to calculate the urinary bladder residence time.

Among the three methods of analysis, the largest differences in residence times occurred between the 2D planar and quadrisectioned methods (Table 1). The 2D planar residence times were higher than the quadrisectioned data for each of the source organs. This difference was magnified in those organs that are asymmetrically localized in either the anterior or posterior aspect of the body (i.e., the heart, kidneys, gallbladder and urinary bladder). With the exception of the lungs, the bisected images provided residence times for source organs that were intermediate to the values obtained from the 2D planar and quadrisectioned images. The residence time of the lungs was unexpectedly higher in the bisected analysis than that in the planar method by a factor of 1.03. This aberration is most likely insignificant and probably occurred due to the difficulty in defining the border between heart and lungs on the 2D planar images. A small amount of activity that was assigned to the lungs on bisected images may have been incorrectly assigned to the heart on the 2D planar images. As expected, the “remainder of body” residence time was lowest for the 2D planar analysis and highest for the quadrisectioned method, due to the remainder’s inverse correlation with the amount of activity in source organs.

For the three methods of analysis, differences in doses to individual organs reflected the differences in their residence times. In comparison to the 2D planar method, the doses for individual organs varied by factors of 0.65–1.06 and 0.6–1.1 for the bisected and quadrisectioned methods, respectively (Table 2). The organs with the highest radiation doses ( $\mu\text{Gy}/\text{MBq}$ ) in the 2D planar image analysis were the gallbladder wall (23), kidneys (20), urinary bladder wall (19) and liver (15). The above organs had the highest doses in the bisected and quadrisectioned image analyses as well. The effective dose obtained from the 2D planar analysis was 4.8  $\mu\text{Gy}/\text{MBq}$ . The greatest difference among doses occurred when the 2D

Table 1  
Residence times (h) of identified source organs

Organ	Human <sup>a</sup>			Monkey <sup>b</sup>
	2D planar	Bisected	Quadrisectioned	2D planar
Brain	0.022±0.004	0.021±0.003	0.019±0.003	0.035±0.012
Gallbladder	0.008±0.003	0.005±0.002	0.004±0.002	–
Heart	0.029±0.003	0.023±0.003	0.019±0.003	0.007±0.001
Kidneys	0.020±0.006	0.013±0.005	0.012±0.005	0.028±0.003
Liver	0.083±0.016	0.081±0.016	0.079±0.016	0.068±0.021
Lungs	0.032±0.002	0.034±0.004	0.031±0.004	0.040±0.011
Urinary bladder	0.026±0.007	0.025±0.007	0.024±0.007	0.082±0.029
Remainder of body	0.259±0.029	0.279±0.027	0.293±0.031	0.218±0.067

<sup>a</sup> Values are mean±S.D. of eight human subjects.

<sup>b</sup> Values are mean±S.D. of three monkey subjects.

Table 2  
Radiation dose estimates for [<sup>11</sup>C](R)-rolipram in standard reference man

Target organ	Human <sup>a</sup>			Monkey <sup>b</sup>
	2D planar (μGy/MBq)	Bisected (ratio to 2D planar)	Quadrisedected (ratio to 2D planar)	2D planar (ratio to human 2D planar)
Gallbladder wall	23.1	0.65	0.6	0.15
Kidneys	19.7	0.96	0.91	2.89
Urinary bladder wall	19.3	0.7	0.62	1.36
Liver	15.2	0.97	0.93	0.80
Heart wall	11.8	0.84	0.74	0.39
Lungs	9.6	1.03	0.94	1.15
Brain	5.2	0.97	0.91	1.60
Adrenals	3.4	0.97	0.97	0.88
Pancreas	3.3	0.98	0.98	0.84
Uterus	2.8	1.02	1.04	1.49
Osteogenic cells	2.8	1.05	1.08	0.90
Total body	2.7	1.01	1.01	0.96
Thymus	2.6	0.99	0.98	0.74
Upper large intestine wall	2.6	1.0	1.03	0.90
Stomach wall	2.5	1.01	1.03	0.85
Small intestine	2.5	1.02	1.05	0.96
Spleen	2.5	0.99	1.01	0.93
Ovaries	2.4	1.04	1.07	1.17
Lower large intestine wall	2.3	1.04	1.07	1.21
Muscles	2.1	1.03	1.06	0.95
Red marrow	2.0	1.02	1.03	0.94
Breasts	1.9	1.03	1.04	0.82
Thyroid	1.8	1.06	1.10	0.89
Testes	1.8	1.05	1.10	1.15
Skin	1.6	1.05	1.08	0.91
Effective dose equivalent	7.8	0.88	0.83	1.17
Effective dose	4.8	0.99	0.95	1.40

<sup>a</sup> Values are mean of eight human subjects.

<sup>b</sup> Values are mean of three monkey subjects.

planar and quadrisedected values of asymmetrically localized organs were compared. Doses for these and all other source organs were always higher in the 2D planar than in the quadrisedected analysis. In contrast, organs that were not designated as source organs often showed slightly higher doses in the bisected and quadrisedected analyses than in the 2D planar method. These differences were due to the fact that more activity was assigned to the “remainder of body” in the bisected and quadrisedected analyses. The effective dose was 1% and 5% lower for the bisected and quadrisedected methods, respectively, compared to the 2D planar analysis.

### 3.2. Monkey biodistribution

Intravenous injection of [<sup>11</sup>C](R)-rolipram produced no significant changes in pulse, respiratory rate or ECG readings. The brain, heart, kidneys, liver, lungs and urinary bladder were all visually identified as source organs on 2D planar images (Fig. 3). Among the organs whose uptake of activity peaked during the course of the emission scans, the liver showed the highest uptake with a peak of 24% injected

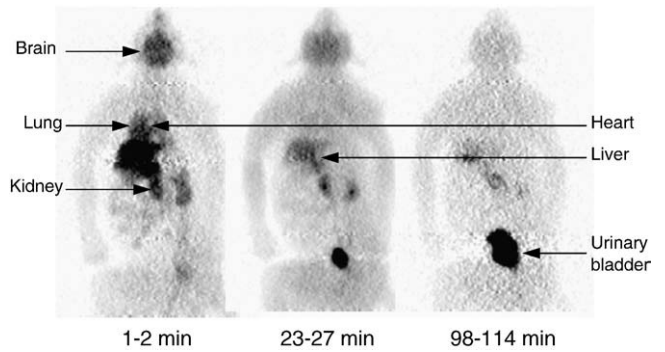


Fig. 3. Series of compressed whole-body 2D planar PET images for one male rhesus monkey. Images were obtained about 1–2, 23–27 and 98–114 min after intravenous injection of 156 MBq [<sup>11</sup>C](R)-rolipram. All three decay-corrected images used the same gray scale (bottom of figure).

activity about 3 min after the injection of [<sup>11</sup>C](R)-rolipram. Average peak uptake in the lungs, kidneys, brain and heart was 7.8%, 7.3%, 7.2% and 3.4% injected activity, respec-

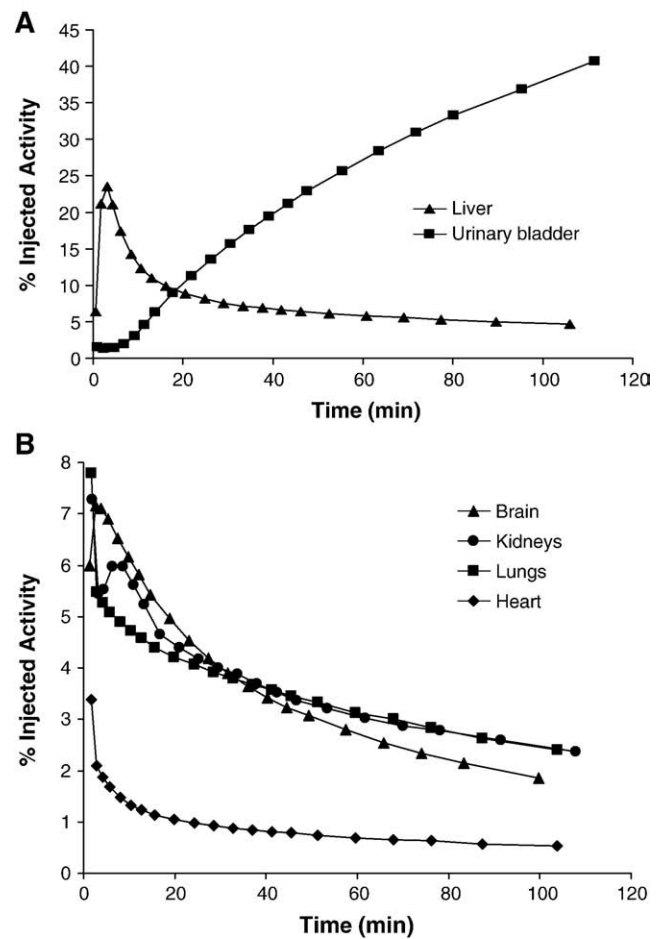
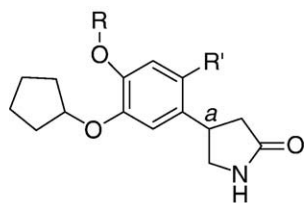


Fig. 4. Mean decay-corrected activity in visually identifiable organs that have high (A) and low (B) uptake after injection of [<sup>11</sup>C](R)-rolipram in two monkeys. A third monkey had similar time–activity curves, but they could not be included in the average of those presented due to differences in scan acquisition times. Activities were determined from 2D planar images.



R =  $^{11}\text{C}$ CH<sub>3</sub>, R' = H, a = R; [ $^{11}\text{C}$ ](R)-Rolipram  
 R = CH<sub>3</sub>, R' =  $^3\text{H}$ , a = R,S; [ $^3\text{H}$ ](R,S)-Rolipram

Fig. 5. Structure of (R)-rolipram showing the position of  $^{11}\text{C}$  used in PET imaging and  $^3\text{H}$  used in clinical pharmacology studies.

tively, all occurring within 10 min of injection (Fig. 4A and B). Although the urinary bladder time–activity curve showed a slight curvature (Fig. 4A), fitting did not converge with either a mono- or biexponential function. Thus, a voiding bladder model was not used to calculate the urinary bladder residence time.

Mean residence times were calculated based on the imaging data acquired from three different monkeys by using the weighting factor described in Section 2 to convert to human values (Table 1). Based on these residence times, the organs with the highest radiation doses ( $\mu\text{Gy}/\text{MBq}$ ) were the urinary bladder wall (57), kidneys (26), liver (12) and lungs (11). The estimated human effective dose from the monkey 2D planar analysis was  $6.6 \mu\text{Gy}/\text{MBq}$ , which was 40% higher than that estimated from human images ( $4.8 \mu\text{Gy}/\text{MBq}$ ).

### 3.3. Percent recovery of injected activity

The recovery of injected activity declined during the scanning of both humans and monkeys. From the beginning to the end of scans in every monkey and in the average of all eight human subjects, the recovery of activity declined by about 4%. Average recovery in both humans and monkeys declined from about 90% to 86%. This loss of radioactivity could have been caused by distribution within the body but outside the field of view (i.e., below the mid-thigh) or possibly by exhaling radioactivity. Krause and Kuhne [19] demonstrated that the *O*-methyl group in rolipram is cleaved during metabolism in humans and in cynomolgus monkeys, though not in rhesus monkeys. We prepared [ $^{11}\text{C}$ ](R)-rolipram with  $^{11}\text{C}$  in this methoxy position (Fig. 5). After cleavage, the radioactive species containing radioactive carbon would likely be rapidly metabolized and exhaled as [ $^{11}\text{C}$ ]CO<sub>2</sub> [20]. Thus, the decreased recovery of radioactivity in humans, but not necessarily rhesus monkeys, could reflect the often overlooked route of pulmonary excretion.

### 3.4. Comparison of monkey and human biodistribution data

The uptake and biodistribution of activity following injection of [ $^{11}\text{C}$ ](R)-rolipram were somewhat similar in monkeys and humans. With the exception of the gallbladder, which was only visible in human subjects, the same source organs were identified in both groups. The overall

human effective dose calculated from the monkey data was 1.4-fold higher than that calculated from the human 2D planar images (Table 2). The greatest differences were seen in the kidneys and brain, which were overestimated in monkeys by factors of 2.9 and 1.6, respectively, while the heart wall and gallbladder were underestimated by factors of 0.39 and 0.15, respectively.

## 4. Discussion

The present study reports the biodistribution and radiation doses of the PDE4 imaging agent [ $^{11}\text{C}$ ](R)-rolipram. Human whole-body PET analyzed with 2D planar images estimated a modest effective dose of  $4.8 \mu\text{Gy}/\text{MBq}$ . The low mass dose of carrier rolipram ( $1.73 \pm 0.46 \mu\text{g}$ ) injected with [ $^{11}\text{C}$ ](R)-rolipram produced no subjective effects and no meaningful changes in laboratory tests, EKG, blood pressure, pulse and respiration rate. Therefore, [ $^{11}\text{C}$ ](R)-rolipram appears safe from both pharmacologic and radiation exposure standpoints.

Uptake of radioactivity was highest in liver for human subjects with a peak value of 21% injected activity about 1 min after injection of [ $^{11}\text{C}$ ](R)-rolipram. Despite this initial uptake of radioligand, liver activity decreased by about 40% within 30 min, and the estimated radiation dose ( $\mu\text{Gy}/\text{MBq}$ ) to the liver (15) was actually lower than that to the gallbladder wall (23), kidneys (20) and urinary bladder wall (19). Collectively, these doses suggest that high levels of excretion occurred via both hepatobiliary and urinary routes. Excretion of radioactivity via the urine was substantial. Urinary bladder uptake (41% injected activity in monkeys and 16% injected activity in humans) was continuing to increase at the end of the scans. However, with only 2 h of data, an estimate of total excretion via urine cannot be made. At 2 h, activity in the urinary bladder of monkeys was just beginning to plateau, whereas that of human was still linearly increasing.

### 4.1. Comparison with pharmacokinetic data

The pharmacokinetics of rolipram has been relatively thoroughly studied in animals and humans as part of its evaluation as an antidepressant medication [19,21–23]. Nevertheless, only limited analogies are possible between these pharmacokinetic data and the current biodistribution study, because different portions of the molecule are monitored and because different lengths of observation are used. Pharmacokinetic studies of rolipram monitored the parent compound itself or monitored radioactivity from tritium in [ $^3\text{H}$ ]rolipram, labeled at position 5 of the phenyl ring [19] (Fig. 5). In contrast, we measured radioactivity from  $^{11}\text{C}$  on the *O*-methyl group (Fig. 5). The prior clinical pharmacology studies in humans, rodents and monkeys identified eight major metabolites formed mainly through hydroxylation or cleavage of either ether function [19,22]. In all species, rolipram was almost completely metabolized

within 24 h, and more than 80% of both orally and intravenously administered  $^3\text{H}$  radioactivity was excreted via urine [19,22]. We also found that a sizeable percentage of  $^{11}\text{C}$  radioactivity from intravenously administered [ $^{11}\text{C}$ ](*R*)-rolipram was excreted via urine: at least 41% in monkeys and 16% in humans by 2 h. Nevertheless, we cannot estimate the amount of  $^{11}\text{C}$  that would be excreted in 24 h and could probably not accurately measure the small amount of activity remaining at that late time. Comparisons are made even more difficult to interpret as the relative abundance of different metabolites in urine was not noted in the pharmacokinetic analysis, and we did not perform metabolite analyses in the present study. Thus, although pharmacokinetic evaluations of rolipram and the present whole-body imaging study of [ $^{11}\text{C}$ ](*R*)-rolipram provide partially overlapping data, neither method could completely substitute for the other.

#### 4.2. Comparison of 2D planar, bisected and quadrisected methods

2D planar images slightly overestimated radiation doses to individual source organs in comparison to bisected and quadrisected images. Differences in organ doses were greatest between 2D planar and quadrisected analyses for asymmetrically located organs (i.e., heart, kidneys, gallbladder and urinary bladder). The largest discrepancy among the methods was the dose to the gallbladder (23  $\mu\text{Gy}/\text{MBq}$ ), which was 40% higher for the 2D planar analysis than the quadrisected method. Similar differences among methods of analysis were seen in our laboratory's prior report on a neurokinin type 1 receptor antagonist [ $^{18}\text{F}$ ]SPA-RQ [16]. As noted in that report, the medical significance of the overestimation of individual organ doses is questionable, as the higher values obtained from 2D planar analysis represent more conservative estimates of radiation risk.

Despite differences in organ doses, the overall effective dose, which is commonly viewed as the primary measure of radiation risk, was quite similar for all three analyses. The effective dose ( $\mu\text{Gy}/\text{MBq}$ ) estimated from 2D planar images (4.8) was about 1% higher than the bisected estimate (4.7) and 5% higher than the quadrisected estimate (4.5). These small differences are similar to those seen in our previous report on [ $^{18}\text{F}$ ]SPA-RQ [16], where 2D planar effective dose estimates were 10% higher than minimally compressed thin-slice images. Therefore, the higher, more conservative 2D planar doses are again reasonable estimates of radiation exposure.

In certain cases, a combination of 2D planar, bisected and quadrisected analyses may be most appropriate. As noted previously, the borders of kidneys were often difficult to identify on 2D planar images in the present study. Kidneys were instead identified on posterior bisected images, and more accurately drawn regions were then propagated to the corresponding 2D planar image. This strategy does not appear to have been of great significance in the present study, as the estimated 2D planar dose to the kidney was only 4% and 9% higher than the bisected and quadrisected values,

respectively. Nevertheless, a combination of methods may be indicated for a radioligand highly localized to a small, asymmetrically located organ, especially if another structure overlaps or obscures that organ.

#### 4.3. Monkeys as human surrogate

Biodistribution of [ $^{11}\text{C}$ ](*R*)-rolipram in monkeys poorly estimated human radiation doses to individual source organs and overestimated effective dose by 40%. As in humans, initial uptake of activity was highest in monkey liver with a peak value of 24% injected activity shortly after injection. However, hepatobiliary excretion of radioligand was not evident in monkeys, as the gallbladder was not identifiable. Urinary excretion was far more predominant in monkeys. Peak uptake of activity as a percentage of injected activity in kidneys and urinary bladder was 7% and 41%, respectively, in monkeys. In humans, these values were 4% for the kidneys and 16% for the urinary bladder. As a result of these differences in excretion of radioligand, human radiation doses to the gallbladder were underestimated by a factor of 0.15 in monkeys, and doses to kidneys and urinary bladder wall were overestimated by factors of 2.89 and 1.36, respectively.

Our results question the utility of performing whole-body imaging in monkeys before studying humans. Individual organs of monkeys can be inappropriate models for humans. In addition, the overall measure of exposure, effective dose, can be significantly incorrect but still within the range of values reported for other radioligands. Despite differences in the effective dose of [ $^{11}\text{C}$ ](*R*)-rolipram estimated in monkeys (6.6  $\mu\text{Gy}/\text{MBq}$ ) compared to humans (4.8  $\mu\text{Gy}/\text{MBq}$ ), both values are within the range of those for radioligands used in brain imaging. We recently showed that the average effective dose for 12 other  $^{11}\text{C}$ -labeled tracers is  $6.5 \pm 2.6$   $\mu\text{Gy}/\text{MBq}$  (range, 4.3–14.1  $\mu\text{Gy}/\text{MBq}$ ), with all results based on biodistribution data in humans [24]. In light of the limited agreement of monkey and human dosimetry estimates, one could safely assume that the human effective dose of a given  $^{11}\text{C}$ -labeled radioligand will be less than 14.1  $\mu\text{Gy}/\text{MBq}$  and then calculate an initial starting dose for human studies. The experimenter would determine the actual effective dose from whole-body imaging in humans and thereby obviate any inaccuracies of the monkey as a human surrogate.

## 5. Conclusion

Whole-body PET demonstrated a modest radiation risk profile for the PDE4 imaging agent [ $^{11}\text{C}$ ](*R*)-rolipram with an effective dose of 4.8  $\mu\text{Gy}/\text{MBq}$ . Human 2D planar images provided slightly more conservative (i.e., higher) radiation dose estimates than did bisected and quadrisected methods. Thus, the simpler and less time-consuming 2D planar method appears acceptable to estimate radiation burden for radioligands that are fairly broadly distributed in the body (i.e., not concentrated in organs of high radiation sensitivity).

In the event that small, asymmetrically localized organs exhibit high levels of radioactivity, a combination of 2D planar and bisected or quadrisectioned methods could be used to estimate more accurate radiation doses to individual organs. The distribution of radioactivity to organs of the monkey was different than that in humans and caused a 40% overestimation of the human effective dose.

### Acknowledgments

The Intramural Research Program of NIMH supported this research (project # Z01-MH-002795-04). We thank Jinsong Hong, MS, for synthesis of the radioligand; Janet Sangare, C-RNP, for recruiting the human subjects and assisting with the PET scans; Robert Gladding, CNMT, for scanning the monkeys; the staff of the NIH PET Department for completing PET studies; and PMOD Technologies (Adliswil, Switzerland) for providing its image analysis software.

### References

- [1] Duman RS, Heninger GR, Nestler EJ. A molecular and cellular theory of depression. *Arch Gen Psychiat* 1997;54:597–606.
- [2] Nestler EJ, Aghajanian GK. Molecular and cellular basis of addiction. *Science* 1997;278:58–63.
- [3] D'Sa C, Duman RS. Antidepressants and neuroplasticity. *Bipolar Disord* 2002;4:183–94.
- [4] D'Sa C, Eisch AJ, Bolger GB, Duman RS. Differential expression and regulation of the cAMP-selective phosphodiesterase type 4A splice variants in rat brain by chronic antidepressant administration. *Eur J Neurosci* 2005;22:1463–75.
- [5] Takahashi M, Terwilliger R, Lane C, Mezes PS, Conti M, Duman RS. Chronic antidepressant administration increases the expression of cAMP-specific phosphodiesterase 4A and 4B isoforms. *J Neurosci* 1999;19:610–8.
- [6] Engels P, Fichtel K, Lubbert H. Expression and regulation of human and rat phosphodiesterase type IV isoenzymes. *FEBS Lett* 1994;350:291–5.
- [7] Houslay MD. PDE4 cAMP-specific phosphodiesterases. *Prog Nucl Acid Res Mol Biol* 2001;69:249–315.
- [8] Mizokawa T, Kimura K, Ikoma Y, Hara K, Oshino N, Yamamoto T, et al. The effect of a selective phosphodiesterase inhibitor, rolipram, on muricide in olfactory bulbectomized rats: potential antidepressant activity of rolipram and other selective cyclic adenosine 3',5'-monophosphate phosphodiesterase inhibitors. *Jap J Pharmacol* 1988;48:357–64.
- [9] Wachtel H. Potential antidepressant activity of rolipram and other selective cyclic adenosine 3',5'-monophosphate phosphodiesterase inhibitors. *Neuropharmacol* 1983;22:267–72.
- [10] Fleischhacker WW, Hinterhuber H, Bauer H, Pflug B, Berner P, Simhandl C, et al. A multicenter double-blind study of three different doses of the new cAMP-phosphodiesterase inhibitor rolipram in patients with major depressive disorder. *Neuropsychobiol* 1992;26:59–64.
- [11] Lourenco CM, DaSilva JN, Warsh JJ, Wilson AA, Houle S. Imaging of cAMP-specific phosphodiesterase-IV: comparison of [<sup>11</sup>C]rolipram and [<sup>11</sup>C]Ro 20-1724 in rats. *Synapse* 1999;31:41–50.
- [12] Lourenco CM, Houle S, Wilson AA, DaSilva JN. Characterization of (R)-[<sup>11</sup>C]rolipram for PET imaging of phosphodiesterase-4: in vivo binding, metabolism, and dosimetry studies in rats. *Nucl Med Biol* 2001;28:347–58.
- [13] Tsukada H, Harada N, Ohba H, Nishiyama S, Kakiuchi T. Facilitation of dopaminergic neural transmission does not affect [<sup>11</sup>C]SCH23390 binding to the striatal D<sub>1</sub> dopamine receptors, but the facilitation enhances phosphodiesterase type-IV activity through D<sub>1</sub> receptors: PET studies in the conscious monkey brain. *Synapse* 2001;42:258–65.
- [14] DaSilva JN, Lourenco CM, Meyer JH, Hussey D, Potter WZ, Houle S. Imaging cAMP-specific phosphodiesterase-4 in human brain with R-[<sup>11</sup>C]rolipram and positron emission tomography. *Eur J Nucl Med Mol Imaging* 2002;29:1680–3.
- [15] Fujita M, Zoghbi SS, Crescenzo MS, Hong J, Musachio JL, Lu JQ, et al. Quantification of brain phosphodiesterase 4 in rat with (R)-[<sup>11</sup>C]rolipram-PET. *Neuroimage* 2005;26:1201–10.
- [16] Sprague DR, Chin FT, Liow JS, Fujita M, Burns HD, Hargreaves R, et al. Human biodistribution and radiation dosimetry of the tachykinin NK<sub>1</sub> antagonist radioligand [<sup>18</sup>F]SPA-RQ: comparison of thin-slice, bisected, and 2-dimensional planar image analysis. *J Nucl Med* 2007;48:100–7.
- [17] Stabin MG, Sparks RB, Crowe E. OLINDA/EXM: the second-generation personal computer software for internal dose assessment in nuclear medicine. *J Nucl Med* 2005;46:1023–7.
- [18] Loevinger R, Budinger TF, Watson EE. MIRD primer for absorbed dose calculations. New York: Society of Nuclear Medicine; 1988.
- [19] Krause W, Kuhne G. Biotransformation of the antidepressant D,L-rolipram. II. Metabolite patterns in man, rat, rabbit, rhesus and cynomolgus monkey. *Xenobiotica* 1993;23:1277–88.
- [20] Gunn RN, Ranicar A, Yap JT, Wells P, Osman S, Jones T, et al. On-line measurement of exhaled [<sup>11</sup>C]CO<sub>2</sub> during PET. *J Nucl Med* 2000;41:605–11.
- [21] Krause W, Kuhne G. Pharmacokinetics of rolipram in the rhesus and cynomolgus monkeys, the rat and the rabbit. Studies on species differences. *Xenobiotica* 1988;18:561–71.
- [22] Krause W, Kuhne G, Jakobs U, Hoyer GA. Biotransformation of the antidepressant DL-rolipram. I. Isolation and identification of metabolites from rat, monkey, and human urine. *Drug Metab Dispos* 1993;21:682–9.
- [23] Krause W, Kuhne G, Matthes H. Pharmacokinetics of the antidepressant rolipram in healthy volunteers. *Xenobiotica* 1989;19:683–92.
- [24] Brown AK, Fujita M, Fujimura Y, Liow J-S, Stabin M, Ryu YH, et al. Effects of peripheral benzodiazepine receptor binding in monkey and man on biodistribution and radiation dosimetry of [<sup>11</sup>C]PBR28, a PET radioligand to image inflammation. *J Nucl Med* 2007;48:2072–9.